

## PRECIPITATION HARDENING OPTIMIZATION BY PARTIAL SUBSTITUTION OF Si AND Mg WITH Ge AND Li IN LEAN 6XXX ALLOYS

Eva A. Mørtzell<sup>1,2\*</sup>, Øyvind Paulsen<sup>1</sup>, Calin D. Marioara<sup>3</sup>, Sigmund J. Andersen<sup>3</sup>, Oddvin Reiso<sup>4</sup>, Jostein Røyset<sup>4</sup>, Yanjun Li<sup>2</sup> and Randi Holmestad<sup>1</sup>

<sup>1</sup> *Department of Physics, Norwegian University of Science and Technology (NTNU), N-7491 Trondheim, Norway*

<sup>2</sup> *Department of Materials Science and Technology, Norwegian University of Science and Technology (NTNU), N-7491 Trondheim, Norway*

(\*Corresponding Author: [eva.mortsell@ntnu.no](mailto:eva.mortsell@ntnu.no))

<sup>3</sup> *SINTEF Materials and Chemistry, N-7465 Trondheim, Norway*

<sup>4</sup> *Hydro Aluminium R&D Sunndal, N-6600 Sunndalsøra, Norway*

### ABSTRACT

With the purpose of increasing the extrudability of lean alloys, we reduce levels of the alloying elements Mg and Si in a 6xxx extrusion alloy. To avoid sacrificing strength, we investigate the compensating effect of smaller amounts of lithium and germanium, alone and in combination. Recent studies by atomically resolved high angle annular dark-field scanning transmission electron microscopy (HAADF-STEM) together with density functional theory (DFT) calculations have demonstrated that while Li replaces Mg, Ge substitutes Si in the columns in the hardening  $\beta''$ -phase. Several studies have shown that Ge replaces Si in other precipitates as well, and that both Li and Ge promote precipitation and can improve macroscopic properties, like strength and thermal stability. The scope of the current work has been to investigate and document the combined effect of the two alloying elements. Of the investigated alloys, the one containing both elements displayed highest hardness, corresponding with a significant increase in precipitate number density. We used HAADF-STEM to determine the extent of Li and Ge in the precipitate structures.

### KEYWORDS

Al-Mg-Si,  $\beta''$ , Li, Ge, HAADF-STEM, TEM

## INTRODUCTION

The two most important alloying agents, with respect to age hardening of the 6xxx alloy series, are Mg and Si. In general, 6xxx alloys are formed into their final shapes by rolling or extrusion, before being age-hardened at elevated temperatures around 180°C. The hardening effect during this stage is due to the formation of metastable, semi-coherent, precipitate needles along the three  $\langle 001 \rangle_{Al}$  directions generally following the precipitation sequence (Marioara, Nordmark, Andersen, & Holmestad, 2006):

Supersaturated solid solution  $\rightarrow$  atomic clusters  $\rightarrow$  Guinier-Preston-zones (pre- $\beta''$ ) (Edwards, Stiller, Dunlop, & Couper, 1998) (Marioara, Andersen, Jansen, & Zandbergen, 2001)  $\rightarrow$   $\beta''$  (Andersen, et al., 1998) (Hasting, et al., 2009)  $\rightarrow$   $\beta'$  (Vissers, Huis, Jansen, & H. W. Zandbergen, 2007),  $U1$  (Andersen, Marioara, Vissers, Frøseth, & Zandbergen, 2007),  $U2$  (Andersen, Marioara, Frøseth, Vissers, & Zandbergen, 2005),  $B'$  (Vissers, Marioara, Andersen, & Holmestad, 2008)  $\rightarrow$   $\beta$ , Si (stable)

The most common phase observe at peak hardness conditions is the monoclinic  $\beta''$  phase. With the monoclinic axis  $\mathbf{b}$  along the needle-axis, the cross section plane is defined by parameters  $\mathbf{a}_{\beta''} \parallel \langle 3\bar{2}0 \rangle_{Al}$  and  $\mathbf{c}_{\beta''} \parallel \langle 130 \rangle_{Al}$ , with an angular separation of 105.3°. The recurring (molecular) unit in  $\beta''$  consists of 11-atoms, and is called a  $\beta''$ -eye. Viewed along the needle direction, it consists of a  $Mg_4Si_4$  ring centred about an Al or Mg atom plus two Al outliers (left/right sides in Fig. 3(a)). The ring replaces corners (Mg) and side faces (Si) on an FCC Al-unit cube. The ring centre is interstitial relative to aluminium (e.g. bottom face is pushed into the Al cube centre). The flexible satellite sites, originally determined as Si and Al, frequently adopt Cu, especially at the precipitate/matrix interface (Saito, et al., 2016) (Saito, et al., 2014).

Ge substitutes Si in precipitate structures when added to Al-Mg-Si alloys, and a projected hexagonal Ge-network (hexagonal in projection) with Ge atomic columns, often aligning with  $\langle 001 \rangle_{Al}$ , forms (Bjørge, Marioara, Andersen, & Holmestad, 2010) (Mørtzell, et al., 2015) (Mørtzell, Andersen, Friis, Marioara, & Holmestad, 2017). By replacing some Si with Ge, the initial strength of the alloy can be significantly improved (Mørtzell, et al., 2015).  $\beta''$  often occurs in Al-Mg-Si-Ge alloys, both alone with Ge replacing Si-sites, and as fragments together with disordered parts containing the Ge-network. Two additional stacking variations of  $\beta''$ -eyes have been documented to occur alone or in different combinations in such alloys (Mørtzell, Andersen, Friis, Marioara, & Holmestad, 2017).

Adding Li to Al-Mg-Si alloys reduces the alloy density (Polmear, 2006) and may increase the age-hardening response (Koshino, Kozuka, Hirosawa, & Aruga, 2015). Both atom probe tomography (APT) and high angle annular dark field scanning transmission electron microscopy (HAADF-STEM) show that Li is incorporated in the precipitates. Also with Li addition,  $\beta''$  was the main hardening phase in the alloy system while thermal stability and hardness improved (Mørtzell, et al., 2017). It was discovered that Li prefers (to occupy)  $Mg_3$ -sites in  $\beta''$ -eyes, which was supported by density functional theory (DFT) calculations.

Based on earlier work (Mørtzell, Andersen, Friis, Marioara, & Holmestad, 2017) (Mørtzell, et al., 2017), which has identified Ge to occupy Si-sites and Li to occupy  $Mg_3$ -sites in the  $\beta''$ -eyes, we designed a new alloy with both Li and Ge additions. The scope of this work has been to optimize precipitation by combining these two elements, which separately have proven to enhance precipitation greatly. A combination of both additions might therefore give even better alloy properties.

Precipitate number density and size statistics have been obtained by conventional transmission electron microscopy (TEM) and electron energy loss spectroscopy (EELS). In order to reduce the influence from objective lens defocus and specimen thickness, all alloys were further investigated by atomically resolved HAADF-STEM. In addition HAADF-STEM provides atomic number contrast (Z-contrast), due to the increased probability of scattering to higher angles as the atomic number increases (Yamazaki, Kawasaki, Watanabe, Hashimoto, & Shiojiri, 2002) (Nellist & Pennycook, 1999).

## EXPERIMENTAL

The chemical compositions of the alloys have been measured by inductively coupled plasma atomic emission spectroscopy and is given both in atomic percent (at %) and weight percent (wt %) in Table 1. RX1 is the lean Al-Mg-Si reference alloy included for comparison.

The as-cast alloys were homogenized for 3 hours, then pre-heated to 575°C before extrusion into solid cylinders with 2 cm diameter. The rods were extruded directly into room tempered water. Samples cut perpendicular to the extrusion direction were solution heat-treated in a salt bath at 535°C (Mørtzell, et al., Effects of Germanium, Copper, and Silver Substitutions on Hardness and Microstructure in Lean Al-Mg-Si Alloys, 2015), water quenched to room temperature (RT) and naturally aged for four hours followed by artificial ageing (AA), to peak hardness, at 195°C for 4 hours in an air circulation furnace. Micro hardness (HV) was measured using a Matsuzawa 0.3–20 kg hardness tester, using a 1 kg load.

Table 1. Alloy composition and effective solute ( $S_{\text{eff}}$ )

Alloy	Si	Ge	Mg	Li	Fe	Mn	$S_{\text{eff}}^{\text{a}*}$
RX1 wt%	0.37	-	0.32	-	0.20	0.03	0.64
RX1 at%	0.36	-	0.36	-	0.10	0.015	0.66
RXL1 wt %	0.420	-	0.270	0.013	0.200	0.030	0.65
RXL1 at %	0.404	-	0.300	0.051	0.097	0.015	0.71
RXG2 wt %	0.350	0.10	0.300	-	0.200	0.030	0.70
RXG2 at %	0.340	0.04	0.33	-	0.097	0.015	0.67
RXGL1 wt %	0.360	0.029	0.270	0.010	0.190	0.089	0.62
RXGL1 at %	0.350	0.010	0.300	0.040	0.090	0.040	0.65

<sup>a</sup>Effective solute  $S_{\text{eff}} = \text{Mg} + \text{Si}^* + \text{Ge} + \text{Li}$ . In the alloy designations. Lithium and Germanium are abbreviated 'L' and 'G', respectively.

\*Effective Si available for precipitation ( $\text{Si}^*$ ) is 0.05 wt % less the tabulated amount (Tundal, O.Reiso, Hoff, Dickson, & Devadas, 2012).

TEM specimens were made by cutting thin slices perpendicular to the extrusion direction and mechanically polishing the slices with SiC paper to a thickness of about 100  $\mu\text{m}$ . Disks with a diameter of 3 mm were stamped from the foils and electropolished by using a Struers Tenu-Pol 5 in an electrolyte consisting of one part nitric acid and two parts methanol. The electrolyte was kept at  $-25^\circ\text{C}$  by adding liquid  $\text{N}_2$  throughout the thinning process.

Low magnification TEM images were acquired in a JEOL 2100 operated at 200 kV for RXGL1. For the remaining alloys, a Philips CM30 operated at 150 kV was used to obtain microstructure statistics of precipitates. Parallel electron energy loss spectroscopy (PEELS) has been performed in order to obtain the average thickness of each imaged area. For a full description of the methods behind the statistics presented in Table 2, see (Marioara, Andersen, Zandbergen, & Holmestad, 2005).

The HAADF-STEM images were acquired in a double corrected JEOL ARM200F operated at 200 kV, with 0.08 nm probe size and an inner HAADF collection angle of 50 mrad. For the Li containing alloys, a series consisting of approximately 20 images was taken to correct drift, relative intensities and distortions by use of the SmartAlign software (Jones, et al., 2015).

## RESULTS

Figure 1 shows representative TEM bright field (BF) images of the precipitates from each of the four investigated alloys. Table 2 gives the corresponding statistics. Considering the results in Figure 1 and Table 2, it is evident that the reference alloy, RX1, has a much lower number density of precipitate needles than the other three alloys. By adding only 0.013 wt % Li to the alloy (RXL1), one can observe a

significant refinement of the precipitate microstructure in addition to a large increase in precipitate number density.

Adding only 0.10 wt % Ge to the alloy (RXG2), results in a refinement of the precipitate microstructure and increases the number density. The corresponding hardness also increases significantly when either Li or Ge is added.

Adding both Li and Ge to the alloy (RXGL1), we observe the highest hardness out of the four investigated alloys. The corresponding microstructure has a significantly higher number density as compared to the other three alloys. The needle cross sections and lengths are however similar to RXG2, but the much higher number density for RXGL1 causes the latter to have a significantly higher volume fraction of needles.

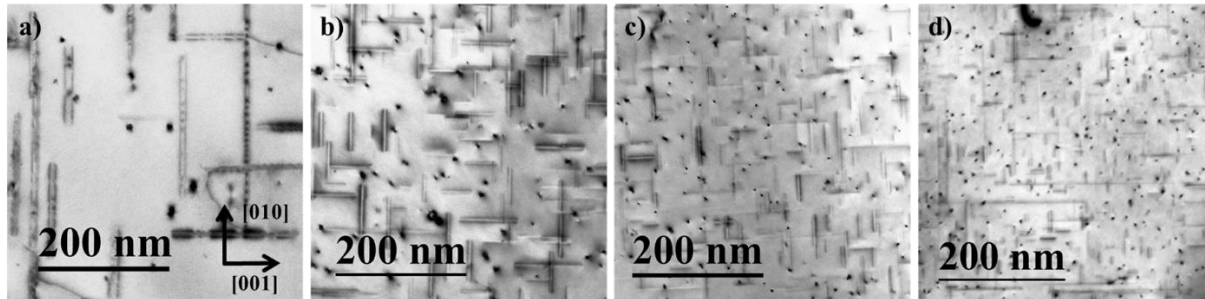


Figure 1. TEM bright field images along  $\langle 001 \rangle_{Al}$  zone, from all four alloys after 4 hours ageing, near peak hardness. a) RX1, b) RXL1 c) RXG2 and d) RXGL1

Table 2. Precipitate statistics after 4h artificial aging at 195°C: Average precipitate cross section, needle length, number density and volume fraction with corresponding errors as measured from TEM micrographs

Alloy	Cross Section [nm <sup>2</sup> ]	Needle Length [nm]	Number Density [#/ $\mu\text{m}^3$ ]	Volume Fraction [%]	HV
RX1	42 ± 4	243 ± 73	170 ± 50	{0.12, 0.19}	50
RXL1	13,1 ± 0,7	56 ± 3	8000 ± 950	{0.53, 0.64}	65
RXG2	7 ± 1	37 ± 1	13200 ± 1400	{0.25, 0.41}	75.5
RXGL1	7.4 ± 0.6	33 ± 1	23000 ± 2500	{0.48, 0.60}	81

The precipitate types have been investigated by HAADF-STEM, and representative cross sections from each alloy are presented in Figure 2. RX1, the reference alloy with only Mg and Si additions, shows a clear majority of well-known phases such as  $\beta''$ ,  $U1$ ,  $U2$  and  $B'$ . In Figure 2 (a), a large  $\beta''$  cross section from RX1 is presented. The Li containing alloy, RXL1 in Figure 2 (b), also exhibits cross sections with  $\beta_2''$  and  $\beta_3''$  fragments. In this alloy, relatively large parts of the cross sections display low intensity, suggesting a higher occupancy of Li.  $\beta''$ -stacking variations occur frequently, with  $\text{Mg}_3$ -sites in the  $\beta''$ -eyes showing lower intensity in HAADF-STEM as compared to RX1. Again, this indicates the presence of Li in  $\beta''$ .

Figure 2 (c) shows a typical cross section in the Ge-added alloy, RXG2. Here a hexagonal network of high intensity columns is observed along the  $\langle 100 \rangle_{Al}$  projection for most of the cross sections. Due to the high Z-contrast and absence of other heavy elements, we infer they contain Ge (Mørtzell, Andersen, Friis, Marioara, & Holmestad, 2017) (Bjørge, Marioara, Andersen, & Holmestad, 2010). The alloy containing both Li and Ge (additions) has a similar variety of cross sections as RXG2, that is, the two dominating features are the hexagonal Ge-network and  $\beta''$  stacking variations. The  $\text{Mg}_3$ -sites in the  $\beta''$ -eyes in RXGL1 do not have significantly lower intensity compared to RX1.

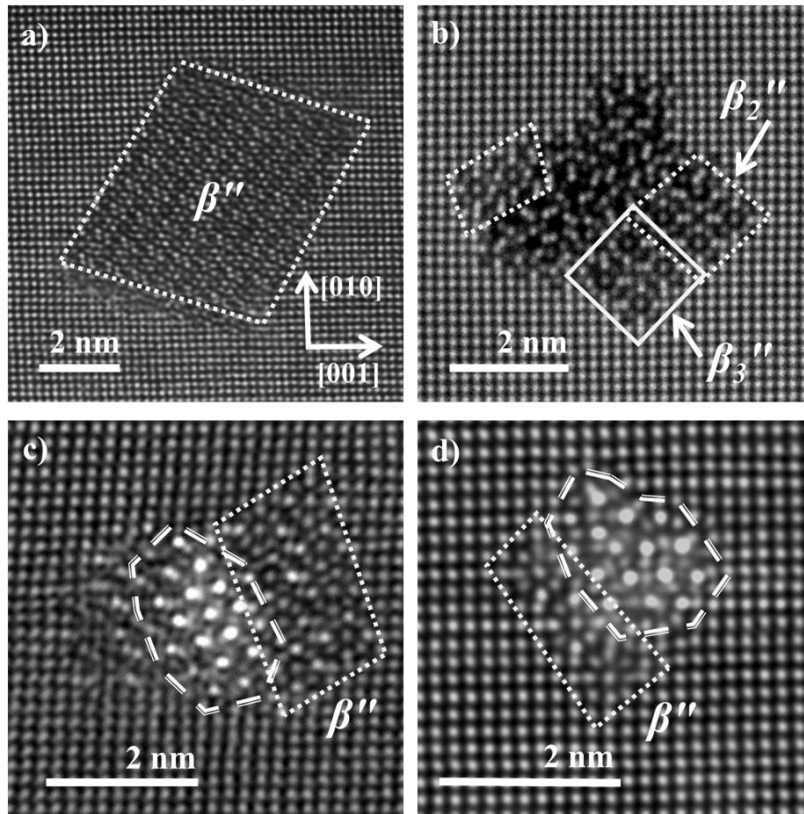


Figure 2. HAADF-STEM images of typical precipitate cross-sections of the four alloys observed in (a) RX1: Dotted rectangle delimiting  $\beta''$ . (b) RXL1: Lower intensity Mg columns show Li substitution. Dotted boxes show regions of  $\beta_2''$ , solid lines demarcate  $\beta_3''$ . (c) RXG2: Precipitate composed of hexagonal Ge/Si network (left) together with  $\beta''$ -regions with Ge occupying  $Si_1$  and  $Si_2$ -sites (right), (d) RXGL1: Precipitate with three  $\beta''$ -eyes (left box) and a part (right dashed figure) with hexagonal Si/Ge network. The Al orientation shown in a) is common for all four images

## DISCUSSION

### Alloy RXL1

Although available solute (in at %) for precipitation is comparable for all four investigated alloys, corresponding precipitate microstructures show strong differences after artificial ageing. Compared to RX1, the Li substitution of Mg in RXL1 strongly refines this microstructure. By the considerable increase in precipitate numbers Li appears to have enhanced formation of ‘good clusters’ during the early stages of precipitation (Torsæter, et al., 2010), an effect which could be linked to a higher Li diffusivity, compared to Mg (Moreau, Allouche, & Knystautas, 1985).

In an earlier HAADF-STEM / DFT study, it was shown that Li replaces Mg-sites in the  $\beta''$  phase, in particular the  $Mg_3$ -sites (Mørtzell, et al., 2017), (see Figure 3 (b)). Cross sections analysed from RXL1 in the current work finds lower intensity corresponding to the same sites, see Figure 2 (b). Li additions do not change the main hardening phase, but refines the precipitate microstructure.

### Alloy RXG2

The partial substitution of Si by Ge gives a further refinement of the precipitate microstructure, as compared to RXL1. In comparison, the mere 0.04 at % Ge increases number of precipitates by almost a factor of 80. Several studies show that Ge should diffuse relatively fast as an impurity in solid aluminium

(Peterson & Rothman, 1969) (Hirano & Fujikawa, 1978). Together with its ability to attract vacancies, this result is faster clustering, and a higher fraction of viable clusters larger than the critical size for further growth into precipitates.

The diamond (D) elements Ge and Si have similar chemical properties, and not surprisingly both occupy  $Si_1$  and  $Si_2$ -sites in the  $\beta''$  phase, see Figure 2 (c). In Al-Mg-Ge alloys, Ge is known to favour structures with more continuous (in projection) hexagonal networks than  $\beta''$ , i.e. like  $\beta'$  and U1 (Bjørge, Marioara, Andersen, & Holmestad, 2010). Thus, hexagonal fragments appear in most precipitate cross sections. Based on the results from HAADF-STEM, a model of the  $\beta''$ -eye in Ge-added alloys is given in Figure 3 (c). Ge has strong effects on the precipitation sequence in Al-Mg-Si alloys (Mørtzell, et al., 2015), and adding a small amount of Ge is in this case no exception. Ge enhances the precipitation kinetics (Mørtzell, et al., 2015) and the hexagonal D-network is similar to the hexagonal Si-network in precipitates associated with over-ageing.

### Alloy RXGL1

The combination of Ge and Li additions results in a significant increase in precipitate number density, even though the available solute for precipitation is the same as for the reference RX1. Compared to Li-substitution only (RXL1), Ge nearly triples precipitate numbers, while it is nearly double that of the Ge-substituted (RXG2) alloy. The strongly refined precipitate microstructure gives RXGL1 the highest hardness of the four alloys, see Table 2. Compared to the reference RX1, the precipitate number density has increased a staggering 13500% (from 170 to 23 000  $\mu\text{m}^{-3}$ ), while the hardness increased 62% (from 50 to 81 HV). The corresponding volume fraction increased from about 0.15% to 0.55%. The intensity at Mg-sites, which is higher for RXGL1 than RXL1, could be due to a lower Li/Mg ratio in the atomic columns. Alternatively, or in addition, the Li atoms could be more evenly distributed among the three different Mg-sites in  $\beta''$ , compared to RXL1. The results in (Mørtzell, et al., 2017) combined with the significant changes in precipitate number density in RXGL1, render it very likely that Li is incorporated in the precipitates also here. A suggested model of the  $\beta''$ -eye is given in Figure 3 (d). Further investigations and DFT-calculations are needed to explain these intensity variations thoroughly.

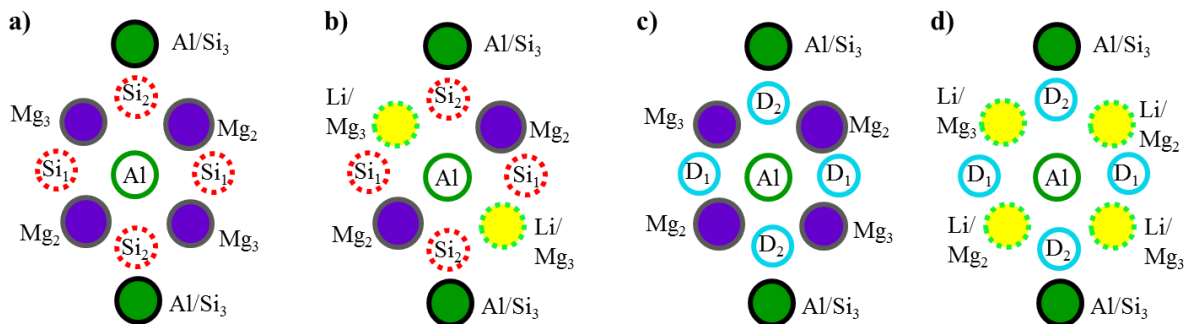












Figure 3. Models of the  $\beta''$ -eyes (molecules) present in the four alloys: (a) Al-Mg-Si reference alloy RX1. (b) Li added alloy RXL1. Low HAADF intensity and DFT calculations suggest Li occupies  $Mg_3$  sites. (c) Ge added alloy RXG2. Higher HAADF intensity at  $Si_1$  and  $Si_2$ -sites indicates Ge occupancy. (d) Suggested model in the alloy with both Li and Ge. D is an abbreviation for ‘diamond element’. See table 3 for an explanation of elements and heights

Table 3. Symbolic representation of elements and their heights in Figure 3

Elements/ Height	Al	Mg	Si	Mixed Li/Mg	Mixed Si/Ge (D)
z = 0.000 m					
z = 0.203 nm					

## CONCLUSIONS

Adding Li to Al-Mg-Si alloys refines and enhances precipitation and consequently improves strength. While the main hardening phase remains unchanged, in the precipitate structures Li partly occupies Mg positions. For the hardening phase  $\beta''$ , the  $Mg_3$  site is most favourable for Li to occupy.

Ge additions have a similar, but stronger refinement / hardness effect than Li. Ge induces fragments with the hexagonal Si/Ge-network in the precipitates, seen in cross sections. Ge also incites fragments in precipitates of other  $\beta''$  stacking variants, favouring  $Si_1$  and  $Si_2$  sites in the  $\beta''$ -eye.

Adding Li and Ge in combination is most favourable out of the four compositions. The strengthening effect after artificial ageing occurs due to the high increase in precipitate number and volume fraction. As in the Ge-added alloy, precipitates comprise fragments of  $\beta''$  and a hexagonal Si/Ge-network. Based on these findings and previous literature, a model of the  $\beta''$ -molecule (eye) is proposed with Li and Mg occupying the  $\beta''$   $Mg_2$  and  $Mg_3$  sites and the diamond elements Si and Ge occupying  $Si_1$  and  $Si_2$ -sites. This work demonstrates that substituting Mg and Si in lean 6xxx alloys with smaller amounts of Li and Ge, improves precipitation and strength considerably.

## ACKNOWLEDGMENTS

The project has been supported through the BIA RolEx project, no. 219371 financed by Hydro Aluminium and the Research Council of Norway, and the Hydro Fond project 'Understanding and multi-scale modelling of early stage precipitation in age hardenable Al-Mg-Si alloys' at Sintef. The STEM work was carried out on the NORTEM JEOL ARM200F, TEM Gemini Centre, NTNU, Norway.

## REFERENCES

- Andersen, S. J., Marioara, C. D., Frøseth, A., Vissers, R., & Zandbergen, H. W. (2005). Crystal structure of the orthorhombic  $U_2-Al_4Mg_4Si_4$  precipitate in the Al-Mg-Si alloy system and its relation to the  $\beta'$  and  $\beta''$  phases. *Mater. Sci. Eng. A*, 390(1-2), 127 - 138.
- Andersen, S. J., Marioara, C. D., Vissers, R., Frøseth, A., & Zandbergen, H. W. (2007). The structural relation between precipitates in Al-Mg-Si alloys and diamond silicon with emphasis on the trigonal phase  $U_1-MgAl_2Si_2$ . *Mater. Sci. Eng. A*, 444, 157 - 169.
- Andersen, S. J., Zandbergen, H. W., Jansen, J., Træholt, C., Tundal, U., & Reiso, O. (1998). The crystal structure of the  $\beta''$  phase in Al-Mg-Si alloys. *Acta Mater.*, 46(9), 3283 - 3298.
- Bjørge, R., Marioara, C. D., Andersen, S. J., & Holmestad, R. (2010). Precipitation in Two Al-Mg-Ge Alloys. *Metal. Mater. Trans. A*, 41, 1907.
- Edwards, G. A., Stiller, K., Dunlop, G. L., & Couper, M. J. (1998). The precipitation sequence in Al-Mg-Si alloys. *Acta Mater.*, 46, 3893 - 3904.

- Hasting, H. S., Frøseth, A. G., Andersen, S. J., Vissers, R., Walmsley, J. C., Marioara, C. D., . . . Holmestad, R. (2009). Composition of  $\beta''$  precipitates in Al–Mg–Si alloys by atom probe tomography and first principles calculations. *J. Appl. Phys.*, *106*.
- Hirano, K., & Fujikawa, S. (1978). Impurity diffusion in Aluminum. *Journal of Nuclear Materials*, *69 & 70*, 564 - 566.
- Jones, L., Yang, H., Pennycook, T. J., Marshall, M. S., Aert, S. V., Browning, N. D., . . . Nellist, P. D. (2015). Smart Align - a new tool for robust non-rigid registration of scanning microscope data. *Advanced Structural and Chemical Imaging*, *1*.
- Koshino, Y., Kozuka, M., Hirosawa, S., & Aruga, Y. (2015). Comparative and complementary characterization of precipitate microstructures in Al–Mg–Si(-Li) alloys by transmission electron microscopy, energy dispersive X-ray spectroscopy and atom probe tomography. *Journal of Alloys and Compounds*, *622*, 765 - 770.
- Marioara, C. D., Andersen, S. J., Jansen, J., & Zandbergen, H. W. (2001). Atomic model for GP-zones in a 6082 Al–Mg–Si system. *Acta Mater.*, *49*, 321 - 328.
- Marioara, C. D., Andersen, S. J., Zandbergen, H. W., & Holmestad, R. (2005). The influence of alloy composition on precipitates of the Al–Mg–Si system. *Metall and Mat Trans A*, *36*(3), 691 - 702.
- Marioara, C. D., Nordmark, H., Andersen, S. J., & Holmestad, R. (2006). Post- $\beta''$  phases and their influence on microstructure and hardness in 6xxx Al–Mg–Si alloys. *J. Mater. Sci.*, *41*, 471 - 478.
- Moreau, C., Allouche, A., & Knystautas, E. J. (1985). Measurements of the diffusion rate of lithium in aluminum at low temperature by elastic. *Journal of Applied Physics*, *58*, 4582 - 4586.
- Mørtzell, E. A., Andersen, S. J., Friis, J., Marioara, C. D., & Holmestad, R. (2017). Atomistic details of precipitates in lean Al–Mg–Si alloys with trace additions of Ag and Ge studied by HAADF-STEM and DFT. *Philosophical Magazine*, *97*(11), 851-866.
- Mørtzell, E. A., Marioara, C. D., Andersen, S. J., Ringdalen, I. G., Friis, J., Wenner, S., . . . Holmestad, R. (2017). The effects and behaviour of Li and Cu alloying agents in lean Al–Mg–Si alloys. *Alloys and Compounds*, *699*, 235-242.
- Mørtzell, E. A., Marioara, C. D., Andersen, S. J., Røyset, J., Reiso, O., & Holmestad, R. (2015). Effects of Germanium, Copper, and Silver Substitutions on Hardness and Microstructure in Lean Al–Mg–Si Alloys. *Metallurgical and Materials Transactions A*, *46*(9), 4369 - 4379.
- Nellist, P. D., & Pennycook, S. J. (1999). Incoherent imaging using dynamically scattered coherent electrons. *Ultramicroscopy*, *78*(1-4), 111 - 124.
- Peterson, N. L., & Rothman, S. J. (1969). Impurity Diffusion in Aluminum. *Physical Review B*, *1*(8), 3264 - 3273.
- Polmear, I. (2006). *Light Alloys, From Traditional Alloys to Nanocrystals*. Oxford UK1: Elsevier.
- Saito, T., Ehlers, F. J., Lefebvre, W., Hernandez-Maldonado, D., Bjørge, R., Marioara, C. D., . . . Holmestad, R. (2014, October). HAADF-STEM and DFT investigations of the Zn-containing  $\beta''$  phase in Al–Mg–Si alloys. *Acta Materialia*, pp. 245 - 253.
- Saito, T., Ehlers, F. J., Lefebvre, W., Hernandez-Maldonado, D., Bjørge, R., Marioara, C. D., . . . Holmestad, R. (2016). Cu atoms suppress misfit dislocations at the  $\beta''$ /Al interface in Al–Mg–Si alloys. *Scripta Materialia*, *110*(1), 6-9.



- Torsæter, M., Hasting, H. S., Lefebvre, W., Marioara, C. D., Walmsley, J. C., Andersen, S. J., & Holmestad, R. (2010). The influence of composition and natural ageing on clustering during preaging in Al-Mg-Si alloys. *J. Appl. Phys.*, *108*, 073527.
- Tundal, U., O.Reiso, Hoff, E., Dickson, R., & Devadas, C. (2012). High Speed Alloys: On the Optimization of 6xxx Alloys. *Proc. 10th International Aluminum Extrusion Technology Seminar, II*, pp. 21 - 33. Miami.
- Vissers, R., Huis, M. A., Jansen, J., & H. W. Zandbergen, C. D. (2007). The crystal structure of the  $\beta'$  phase in Al-Mg-Si alloys. *Acta Mater.*, *55*, 3815 - 3823.
- Vissers, R., Marioara, C. D., Andersen, S. J., & Holmestad, R. (2008). Crystal structure determination of the  $\beta'$  phase in Al-Mg-Si alloys by combining quantitative electron diffraction and ab-initio calculations. *Proceedings ICAAI1, 2*, pp. 1263 - 1269. Aachen.
- Yamazaki, T., Kawasaki, M., Watanabe, K., Hashimoto, I., & Shiojiri, M. (2002). Effect of small crystal tilt on atomic-resolution high-angle annular dark field STEM imaging. *Ultramicroscopy*, *92*(3-4), 181 - 189.